

Limits on the fluctuating part of y -type distortion monopole from Planck and SPT results

Rishi Khatri,^a Rashid Sunyaev^{a,b,c}

^aMax Planck Institut für Astrophysik
, Karl-Schwarzschild-Str. 1 85741, Garching, Germany

^bSpace Research Institute, Russian Academy of Sciences, Profsoyuznaya 84/32, 117997 Moscow, Russia

^cInstitute for Advanced Study, Einstein Drive, Princeton, New Jersey 08540, USA

E-mail: khatri@mpa-garching.mpg.de

Abstract. We use the published Planck and SPT cluster catalogs [1, 2] and recently published y -distortion maps [3] to put strong observational limits on the contribution of the fluctuating part of the y -type distortions to the y -distortion monopole. Our bounds are $5.4 \times 10^{-8} < \langle y \rangle < 2.2 \times 10^{-6}$. Our upper bound is a factor of 6.8 stronger than the currently best upper 95% confidence limit from COBE-FIRAS of $\langle y \rangle < 15 \times 10^{-6}$. In the standard cosmology, large scale structure is the only source of such distortions and our limits therefore constrain the baryonic physics involved in the formation of the large scale structure. Our lower limit, from the detected clusters in the Planck and SPT catalogs, also implies that a Pixie-like experiment should detect the y -distortion monopole at $> 27\text{-}\sigma$. The biggest sources of uncertainty in our upper limit are the monopole offsets between different HFI channel maps that we estimate to be $< 10^{-6}$.

Keywords: cosmic background radiation, cosmology:theory, early universe

Contents

1	Introduction	1
2	The full sky map of y-type distortion and masks	3
2.1	Comparison with Planck maps	4
3	Upper limits on the average y-distortion	5
3.1	Effect of systematic offsets between channels, validation with FFP6 simulation and with lower resolution maps	7
4	Lower limits on the average y-distortion from the Planck and SPT cluster catalogs	9
5	Conclusions	10

1 Introduction

The Planck experiment [4] is the first full sky experiment after COBE (Cosmic Background Explorer) [5, 6] covering the entire CMB spectrum (the blackbody peak, the Rayleigh-Jeans and the Wien regions) with high sensitivity. The wide frequency coverage combined with the unprecedented sensitivity of Planck allows us to detect and separate the y -type distortion [7] over the whole sky and Planck collaboration as well as other groups have already created the maps of y -type distortion from Planck data [8, 9]. The y -type distortion spectrum is given by [7]

$$\Delta I_\nu = \frac{2h\nu^3}{c^2} \frac{xe^x}{(e^x - 1)^2} \left[x \left(\frac{e^x + 1}{e^x - 1} \right) - 4 \right], \quad (1.1)$$

where $x = h\nu/(k_B T_{\text{CMB}})$, h is the Planck constant, k_B is the Boltzmann constant, $T_{\text{CMB}} = 2.725$ is the CMB temperature and c is the speed of light. The y -type distortion has negative intensity, compared to the background CMB, at $\nu < 217\text{GHz}$ and positive intensity at $\nu > 217\text{GHz}$. The Planck experiment has channels covering both regions as well as at the null (217 GHz). The South Pole Telescope (SPT) and the Atacama Cosmology Telescope (ACT) cover only the negative region and the null at present but at much higher angular resolution of $\sim 1'$ [2, 10]. The ACT experiment has also observed at 277 GHz and results including this channel should become available in the near future [11].

Planck and other CMB anisotropy experiments measure the changes in the brightness as they scan the sky and are insensitive to the invariant part of the signal. The y -type distortion present in the Planck maps is therefore expected in the standard cosmology to be solely from the Compton scattering of blackbody CMB photons by the hot electrons present in the clusters and groups of galaxies and hot filaments [12], the result of cosmological structure formation. Since the electrons are hotter than the CMB, Compton scattering results in transfer of energy from electrons to photons, up-scattering the photons from the Rayleigh-Jeans part to the Wien region of the spectrum. The result is a decrease in the intensity of the CMB in the Rayleigh-Jeans part and an increase in the Wien region of the CMB spectrum resulting in the characteristic spectrum of the y -type distortion.¹ The y -type distortion has been used by the SPT (South Pole Telescope), ACT (Atacama Cosmology Telescope) and Planck to discover hundreds of new clusters in addition to studying the physics of known clusters discovered optically or through x-rays [14–21].

¹A detailed review of the various aspects of Compton scattering can be found in [13].

In the future we expect to have experiments such as Pixie (Primordial Inflation Explorer [22]) or PRISM (Polarized Radiation Imaging and Spectroscopy Mission [23]) sensitive to the absolute brightness of the sky and not just the changes in brightness as they scan the sky. These experiments are expected to be 3-4 orders of magnitude more sensitive than COBE-FIRAS (Far Infrared Absolute Spectrophotometer) [24, 25]. These experiments would in particular measure the average y -type distortion or the monopole on the sky improving by many orders of magnitude the current COBE-FIRAS upper limit of $y < 1.5 \times 10^{-5}$ [5].

However since we already have multi-frequency experiments such as Planck and SPT which are more sensitive than COBE-FIRAS and DMR (Differential Microwave Radiometer), it is an interesting question to ask if we can already put better limits on the y -type distortion monopole? The answer turns out to be yes and we use Planck and SPT data to put both upper and lower limits on the y -distortion monopole. This is possible because the y -type distortion from the large scale structure is a strictly positive very inhomogeneous signal with a non-varying part that is very small compared to the part which varies on the sky. Therefore the contribution to the monopole or the average y -type distortion from the invariant part, to which the experiments such as Planck and SPT are insensitive, is expected to be negligible compared to the contribution from the fluctuating part of the y -type distortions, at least in standard cosmological model without any new physics. In the standard cosmological model, there are two main contributors to the invariant part of the y -type distortion.

The first is the dissipation of sound waves before and during recombination known as Silk damping [26–29] due to photon diffusion and free streaming and results in an exponentially decaying anisotropy spectrum in the CMB. This decrease in the power in sound waves on small scales during the epoch of recombination has already been measured by SPT, ACT and Planck [30–32]. This energy which disappears from the CMB anisotropies appears in the CMB monopole as spectral distortions [33–35]. At $z \lesssim 10^4$ the distortion is a y -type distortion while at higher redshifts there is thermalization of the distortions towards the equilibrium Bose-Einstein spectrum resulting in the intermediate and μ -type distortions [33, 36–44]. Since the Universe in the standard model is statistically homogeneous and Gaussian, the sound waves on small scales have the same amount of power everywhere. Therefore we expect that the same amplitude of distortions would be created everywhere, i.e. we would have an invariant contribution to the y -distortion monopole. There will be a small difference in different parts of the Universe because of the cosmic variance which we can neglect. We should mention that in the presence of non-Gaussianity we can have a spatially varying distortion since non-Gaussianity can cause the small scale power to vary from place to place [45–47]. The invariant y -type distortions coming from the Silk damping are expected to be $y^{\text{Silk damping}} \sim 4 \times 10^{-9}$ [34] in the standard Λ CDM cosmological model. Any non-standard energy release during the recombination, which may also create y -type distortions, would also delay recombination and therefore change the CMB anisotropy power spectrum. Any energy release between recombination and reionization is therefore already tightly constrained by the CMB anisotropies [21, 42, 48–52] and the resulting y -type distortion is constrained to be sub-dominant compared to the Silk damping signal.

The second homogeneous contribution is expected to come from reionization at $z \gtrsim 6$. We expect the temperature of gas during the reionization to be $\sim 10^4$ K [53] and with optical depth through reionization of $\tau \sim 0.07$ [21], we expect $y^{\text{Reionization}} \approx \tau T_e / m_e \sim 10^{-7}$ [22].

The fluctuating part on the other hand is expected to be dominated by the contributions from clusters [54, page 15] and groups of galaxies and warm hot intergalactic medium (WHIM) [55, 56]. The contribution from the peaks in the large scale structure and the effect of baryonic physics to the y -type distortion fluctuations has been studied by many groups using numerical simulations as well as analytically [57–68]. The predictions for the average distortion from this fluctuating component range from $y = 10^{-6} - 3 \times 10^{-6}$ [57–62, 64, 66, 68] with majority of simulations leaning towards

$\gtrsim 2 \times 10^{-6}$. This average distortion is sensitive to baryonic physics, in particular to any mechanism that can inject energy into the intergalactic medium. These predictions are the ones that the Planck experiment is sensitive to and are possible to test with the current data.

In addition to the anisotropic contribution to the y -distortion from the large scale structure, we also have contribution from the hot gas in our vicinity. Our Solar system is embedded in a local cavity or bubble of $s \approx 40 - 130$ pc size filled with hot ionized gas with temperatures $\approx 10^6$ K and pressure of $P/k_B \approx 1.5 \times 10^4 \text{ cm}^{-3} \text{ K}$ [69]. This implies a local y -type distortion from our vicinity of $y = \sigma_T P d / (m_e c^2) \approx 5 \times 10^{-10}$, where σ_T is the Thomson scattering cross section and m_e is the electron mass. Our galaxy is also surrounded by a hot halo of ionized gas belonging to the warm hot circumgalactic medium and the local group medium with temperature $\approx 2 \times 10^6$ K and electron density $n_e \approx 2 \times 10^{-4} \text{ cm}^{-3}$ extending to ~ 72 kpc [70] giving $y \sim 5 \times 10^{-9}$. These small local contributions may be detectable by future experiments and could be separated from the cosmological y -distortion owing to their characteristic anisotropic signature on the sky.

2 The full sky map of y -type distortion and masks

Planck collaboration maps [8] of the y -type distortion created using the internal linear combination methods are now publicly available and use two different internal linear combination (ILC) algorithms MILCA (Modified ILC Algorithm) [71] and NILC (Needlet ILC) [72]. We will use the maps of y -type distortion constructed using the Planck HFI channels in [3] using a different method. These maps are constructed using the linearized iterative least-squares (LIL) parametric model fitting scheme proposed in [73]. We reproduce the y -map from [3] in Fig. 1. The well known clusters can easily be spotted on the map. Approximately 14% of the sky most contaminated by the dust and CO emission has been masked in the map.

An advantage of the parametric model fitting is that it gives a quantitative estimate of how good the model fits the data in the form of χ^2 . This information was used in [3] to construct a mask which masks the regions on the sky worst affected by the carbon-monoxide (CO) emission, the main contaminant for the y -distortion signal.

The Planck catalog was also revisited in [3] and clusters and cluster candidates where the y -type distortion signal should be free of CO contamination were identified. We will use this CO mask and the clean sample of clusters to put reliable upper and lower limits on the average y -type distortion. We will try to be conservative everywhere, so that small amount of remaining contamination would always expand our limits. We consider the limits derived in this ultra-conservative way to be the hard limits and the probability that these limits are violated should be vanishing. In calculating the upper limit we will directly average the y -type distortion in the pixels in y -map in real space. We refer the reader to [73] for details of our component separation method and to [3] for details of the construction of the y -type distortion map, CO mask and identification of clean clusters. An important feature of our algorithm is nested model selection. We fit a 3 parameter CMB+dust model as well as a CMB+dust+ y model to every pixel. The difference in χ^2 (or $-2 \ln(\text{Likelihood})$) for the 3 parameter and 4 parameter model has a χ^2 distribution with one degree of freedom. We set a threshold in the χ^2 difference for the two fits, $\Delta\chi^2$, for the acceptance of the extra y parameter. If the improvement in χ^2 by adding the extra y -type component to the sky emission model is larger than the threshold $\Delta\chi^2$, we accept that the y component is present and take the best fit amplitude. If the improvement is smaller than the threshold we reject the y -type component and set the y amplitude in that pixel to zero. A $\Delta\chi^2 = 0$ threshold would imply no model selection and accepting the y -type component everywhere while thresholds of 1.6, 2.7, 3.8 imply that there is 20, 10, 5% probability respectively that we except the 4 parameter model with y component when the fourth y -component is in fact absent i.e. these

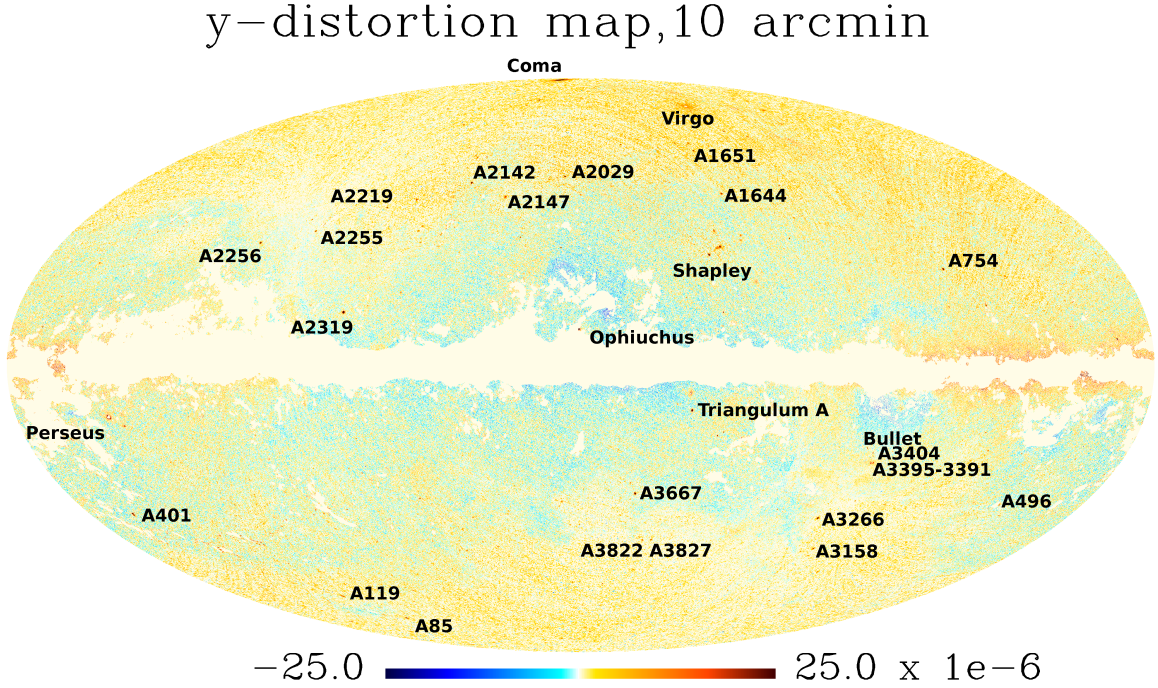


Figure 1. Map of y -type distortion at $10'$ resolution constructed from the lowest four Planck HFI channels in [3].

are the probabilities for the false detection of y -type signal. Higher thresholds would therefore result in cleaner y -maps with the price that some of the below noise y -signal would also be lost. The map shown in Fig. 1 corresponds to $\Delta\chi^2 = 3.8$.

In addition to the Galactic CO emission, the CO emission lines from external galaxies form a diffuse background. This background, integrated over all redshifts, is expected to contribute $\sim 1 \mu\text{K}$ to Planck frequency channels at 100 GHz and above with an almost flat spectrum [74]. The variation with frequency in the redshift integrated spectrum, which is relevant for contamination to the y -distortion, should be even smaller, of order $0.1 \sim \mu\text{K}$ and therefore the contamination to the average y -type distortion of $< 10^{-7}$.² This is a factor of 20 smaller than the upper limit we will get and we can neglect it. Note that the diffuse extragalactic background can give either positive or negative contamination to the y -distortion depending on its exact spectral shape. The galactic CO emission on the other hand, with the canonical line ratios that we have assumed, always gives a positive contamination and will bias our upper limits towards higher values. The strongest contaminant for us is the Galactic CO and dust emission and we will focus on these from now on.

2.1 Comparison with Planck maps

We show in Fig. 2 the probability distribution function (PDF, $P(y)$) of our map calculated with LIL algorithm for $\Delta\chi^2 = 0.0$ and compare it with the MILCA and NILC maps in Fig. 3 for 51% sky fraction (masks are defined in the next section). Also shown are the $P(y)$ when all clusters and cluster candidates in the second Planck cluster catalog are masked. We see in Fig. 2 the skewness in the PDF compared to the symmetric and Gaussian noise PDF, as predicted by [76], from the non-Gaussian

²For Planck 100 GHz channel the conversion from y to brightness temperature K_{CMB} units is $T_{100 \text{ GHz}} = -4.031y$ [75].

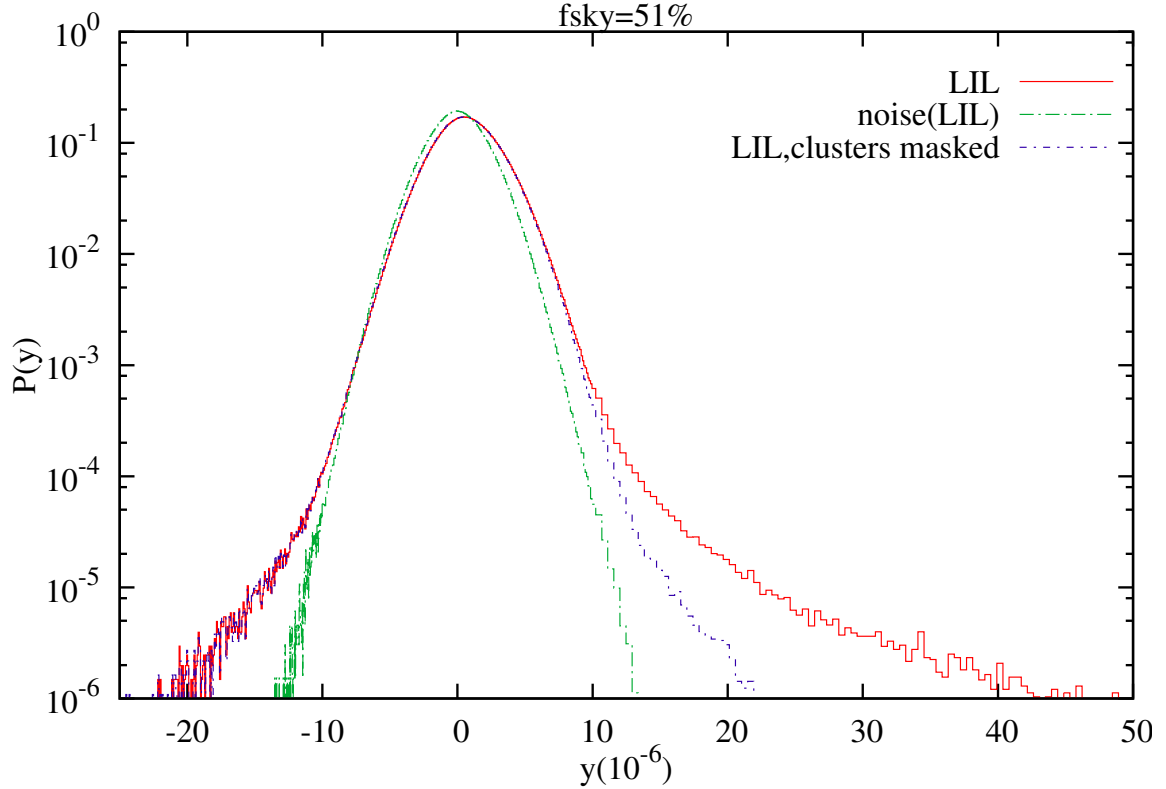


Figure 2. The PDF of our y -distortion map calculated with LIL algorithm for the same 51% of the sky.

y -distortion signal not only in the far tail coming from massive clusters, but also at small y near the center, coming from unresolved clusters and groups of galaxies. All maps in Fig. 3 agree in the positive tails of the distribution which are dominated by the detected clusters. The LIL map has larger noise (calculated from the half ring half difference maps) compared to the MILCA and NILC maps. The width of the MILCA and NILC distributions are however significantly wider than their noise distributions indicating that their maps are probably dominated by contamination while our maps are dominated by noise. The most significant difference in our maps and Planck maps is the absence of positive skewness at small values of y in the MILCA and NILC maps. We expect this skewness if there was y -signal present in the maps below the pixel noise level in the maps. This is probably because the Planck ILC based algorithms explicitly remove the monopole, the very signal we are interested in. We therefore cannot use MILCA and NILC maps to estimate the average y -distortion signal and will only present results from LIL maps. The negative tails, representing galactic and radio source contamination, are slightly larger in case of LIL. However the contribution of these tails to our average y -signal is negligible since their probability is $< 10^{-3}$ compared to the peak. The average y -signal corresponds to the integration over the PDF and gets most of the contribution from near the peak of the PDF at $|y| \sim \text{few} \times 10^{-6}$. We will also quote ultra-conservative values, integrating over only the positive half of the PDF explicitly ignoring the negative contamination tail.

3 Upper limits on the average y -distortion

We will use the y -map and CO masks to estimate the average y -type distortion or the monopole. We have seen in the previous sections that we should expect non-negligible contamination from dust and

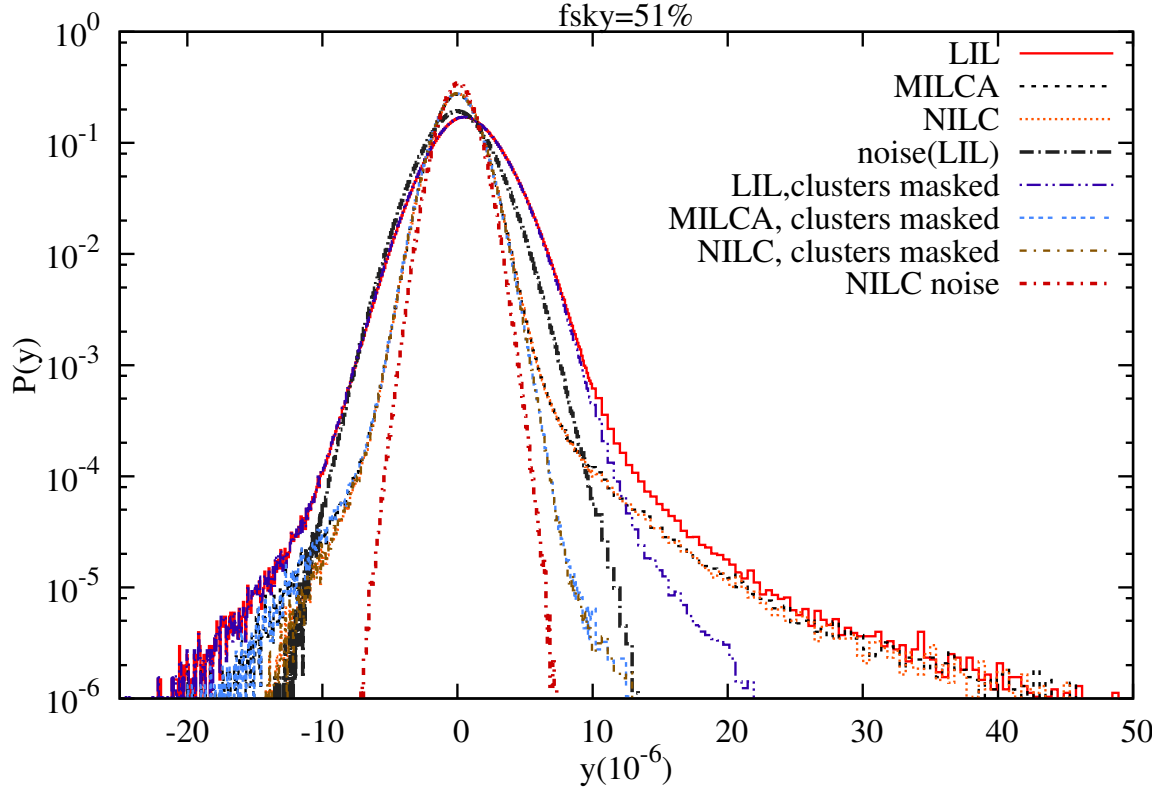


Figure 3. The PDF of LIL, NILC, and MILCA y -maps for the same 51% of the sky. Note that the difference from the PDF published in [8] is because they applied additional filtering to their maps before calculating the PDFs while we plot the unfiltered PDFs.

CO emission in the y -map, especially for pixels where no cluster is detected. Therefore even though it is trivial to calculate the y -distortion from the y -map with statistical error that should be extremely small owing to the averaging over the millions of pixels in the whole sky, the systematic error is much harder to estimate. We will therefore take a conservative approach and instead of giving the error bar at some number of σ , we will try to put a hard upper bound so that the probability that the signal would exceed our upper bound is vanishing. We will validate our results using the FFP6 simulations [77].

We augment our minimal 86% mask using the 545 GHz channel to get successively cleaner and cleaner portions of the sky. Note that unlike the non-zero low order multipoles, for the monopole we do not need a large fraction of the sky and we should expect the monopole to be same in different small patches of the sky for a statistically homogeneous and isotropic Universe. We also analyze the maps generated with different nested model selection thresholds of $\Delta\chi^2 = 0, 1.6, 2.7, 3.8$ to verify how much signal is lost by our model selection procedure, $\Delta\chi^2 = 0$ means no model selection and we fit for the y -distortion component everywhere. Even though we have taken care to mask strong radio sources which appear as negative y sources in the y -map, there will still be some sources below our thresholds that would remain in the map. There is of course positive foreground contamination also, mostly from the residual CO emission, the positive and negative contamination is not expected however to completely cancel each other. There are two ways to handle these pixels when we are interested in the upper bounds. A *conservative* approach would be to set all negative pixels to zero and then average over all the pixels. This procedure would bias our results towards higher values of y

$\Delta\chi^2$	0.0 average — Ucons.	1.6 average — Ucons.	2.7 average — Ucons.	3.8 average — Ucons.
81% sky	0.49 — 2.32	0.53 — 0.95	0.56 — 0.94	0.57 — 0.94
w/o clusters	0.44 — 2.28	0.50 — 0.91	0.52 — 0.91	0.53 — 0.91
71% sky	0.57 — 2.26	0.60 — 0.96	0.62 — 0.96	0.64 — 0.96
w/o clusters	0.52 — 2.22	0.56 — 0.93	0.59 — 0.93	0.60 — 0.92
61% sky	0.62 — 2.25	0.67 — 1.00	0.70 — 0.99	0.71 — 0.99
w/o clusters	0.57 — 2.21	0.64 — 0.96	0.67 — 0.96	0.68 — 0.95
51% sky	0.66 — 2.24	0.75 — 1.03	0.79 — 1.02	0.80 — 1.02
w/o clusters	0.62 — 2.20	0.72 — 1.00	0.75 — 0.99	0.77 — 0.99
41% sky	0.68 — 2.22	0.82 — 1.06	0.86 — 1.05	0.88 — 1.05
w/o clusters	0.63 — 2.18	0.79 — 1.03	0.83 — 1.02	0.85 — 1.01
31% sky	0.65 — 2.16	0.87 — 1.08	0.92 — 1.06	0.95 — 1.06
w/o clusters	0.60 — 2.12	0.83 — 1.04	0.88 — 1.03	0.91 — 1.02

Table 1. Values of y -distortion monopole amplitude $\langle y \rangle \times 10^6$. Both the average values (average) and Ultra-conservative upper bounds (Ucons.) are presented.

as the positive noise fluctuations are still added to the signal. An *ultra-conservative* approach would be to mask or completely ignore the negative pixels and average only the positive pixels completely avoiding the dilution in signal from the negative pixels. In what follows we take the ultra-conservative approach. The resulting y -type monopole for different combinations of above mentioned analysis procedures is summarized in Table 1. We will label the average y when keeping the negative values as *average estimate* and results when masking negative pixels as *Ucons. estimate*. The conservative values of course lie between these two extremes.

There is a small systematic variation with the changing sky fraction and $\Delta\chi^2$, which is expected, in addition to a jump when the model selection is turned on. The fact that the changes from $\Delta\chi^2 = 1.6$ to 3.8 are very small gives us confidence that our model selection is not throwing away too much signal along with the contamination. In particular both the average and ultra conservative values converge towards $\langle y \rangle = 1.0 \times 10^{-6}$ with the decreasing sky fraction and increasing $\Delta\chi^2$ signaling the decrease in foreground contamination. We therefore take $\langle y \rangle = 1.0 \times 10^{-6}$ as our best estimate for the average y -type distortion and take the $\Delta\chi^2 = 0.0, 31\%$ sky fraction value of 2.2×10^{-6} as hard upper bound. It is clear from the table that this is a very conservative bound and we expect that the probability that the average y -type distortion will exceed this value is vanishing. We note that this bound is a factor of 6.8 times stronger the COBE 95% upper limit of 15×10^{-6} [5]. Our limits of course only apply to the fluctuating contribution whereas COBE-FIRAS limits are more generally applicable. We should also mention that for $\Delta\chi^2 = 0.0, 31\%$ sky fraction the conservative limit (see above) is 1.3×10^{-6} close to our best estimate.

We also note that the contribution of clusters from the Planck catalog outside our masks are consistent across the table at $\langle y \rangle_{\text{clusters}} \approx 4 \times 10^{-8}$ and this provides a strong lower limit to the y -type distortion. We will compare this limit with one derived directly from the Planck and SPT cluster catalogs in the next section.

3.1 Effect of systematic offsets between channels, validation with FFP6 simulation and with lower resolution maps

The FFP6 simulations simulate the nominal Planck sky and therefore have higher noise compared to the Planck full mission. Nevertheless we can use the FFP6 simulations to answer the following

	100 GHz	143 GHz	217 GHz	353 GHz
offset (μK)	-3	-3	+5	+23
average y ($\times 10^{-6}$)	0.66	1.92	3.0	-0.39
Ucons. y ($\times 10^{-6}$)	2.2	2.76	3.46	1.83

Table 2. Effect of introducing systematic offsets in one channel at a time. The signs of offsets are chosen to be in the same direction as the y -distortion signal. Note that for the 353 GHz channel, the offset is getting absorbed in the other components and y -distortion signal compensates by going in the direction opposite than expected.

question: Do the foregrounds bias our results towards higher or lower values of y . We have repeated our analysis on the FFP6 simulations which have an input average y of $\approx 3.9 \times 10^{-7}$. Our output y -map has $\langle y \rangle = 4.5 \times 10^{-6}$ corresponding to the ultra-conservative upper limit on 31% sky and no model selection and $\approx 2.8 \times 10^{-6}$ corresponding to the $\Delta\chi^2 = 3.8$. These values are considerably higher compared to our values on the real sky and the true value.

The main reason is that in the FFP6 simulations there are offsets present of order $10 - 30 \mu K$ between the maps which give an almost constant monopole y -signal over the whole sky in our reconstructed y map. This offset contribution, which is positive y -monopole, is really what we are measuring as the average y . To test this, we remove the relative offsets from the FFP6 channel maps estimated from the CMB only channel maps. After removing the rough offsets we get ultra conservative limits of $\langle y \rangle = 1.64 \times 10^{-6}$ and 1.0×10^{-7} for $\Delta\chi^2 = 0.0$ and 3.8 respectively. Thus with and without model selection values nicely bracket the true value of $\langle y \rangle = 3.9 \times 10^{-7}$.

For the real data the offsets have been estimated and removed in the released maps [78]. We also removed the CIB monopole that is added to the released Planck maps together with the best estimates of the residual dipoles [79]. If we do not remove the CIB monopoles, we get much higher values of $\langle y \rangle = 4.1 \times 10^{-6}$ and 2.6×10^{-6} for $\Delta\chi^2 = 0.0$ and 3.8 respectively. The maximum estimated uncertainty in the 100 GHz, 143 GHz and 217 GHz channels for the residual offsets is $3 - 5 \mu K$ and it is $23 \mu K$ for the 353 GHz channel [80] and these are the biggest source of uncertainties for our upper limit. We re-run our calculations after adding offsets corresponding to these uncertainties to one channel at a time. The results for $\Delta\chi^2 = 0.0$ and sky fraction $f_{\text{sky}} = 31\%$ are tabulated in Table 2. We therefore expect the maximum error in our y -estimate to be of order $\sim 10^{-6}$ assuming that the offsets do not completely mimic the y -distortion. If the offset errors are random they will partially cancel each other and we should expect the actual error to be smaller.

The FFP6 simulations do not contain diffuse emission from the WHIM [56] that we expect in the real sky. If such diffuse emission is present, it should be possible to place better limits on the diffuse emission by rebeaming the maps to a bigger beam and redoing the analysis. We do this for the real full mission maps at $30'$ and $60'$ resolution. Note that once we are at such low resolutions it no longer makes sense to do model selection since the signal will be spread out over large areas. We therefore turn-off the model selection (i.e. set $\Delta\chi^2 = 0$) and redo the analysis as in the previous section. For $30'$ resolution we get a conservative $\langle y \rangle = 4 \times 10^{-7}$ and an ultra-conservative value of 7.4×10^{-7} . The corresponding values for the $60'$ resolution are 2.6×10^{-7} and 5.4×10^{-7} . There is therefore a trend towards lower values with increase beam size. For these large beams however there is not sufficient control over the foregrounds which also spread out. We therefore use the smallest average $\Delta\chi^2 = 0$, $f_{\text{sky}} = 31\%$ and largest average value for $\Delta\chi^2 = 3.8$, $f_{\text{sky}} = 31\%$ from Table 1 to give our best estimate for average y to be $7 \times 10^{-7} \leq \langle y \rangle \leq 10^{-6}$. This discussion also shows the difficulty of actually measuring the average y -type distortion in the Planck maps and this is the reason we opt instead to put conservative upper and lower bounds.

sample	Planck				SPT	
	all	S/N> 6	clean	clean(S/N> 6)	$3\theta_c$	$5\theta_c$
$z \leq 0.3$	0.038	0.029	0.033	0.025	0.0073	0.010
$z > 0.3$	0.019	0.0074	0.0099	0.0038	0.021	0.030

Table 3. Average values of y -distortion monopole amplitude $\langle y \rangle \times 10^6$ calculated from the Planck and SPT cluster catalogs [1, 2]. We divide the samples into low redshift and high redshift samples at $z = 0.3$. The Planck and SPT clusters give comparable contributions to the average y -distortion.

4 Lower limits on the average y -distortion from the Planck and SPT cluster catalogs

There are already more than 1000 clusters detected by Planck and SPT and available as catalogues. The average y distortion of course includes contribution from these clusters and therefore we can use these catalogs to provide a hard lower bound on the average y distortion. We use both the Planck and SPT catalogs since they are complimentary. Planck is very good at detecting large nearby clusters while SPT is more efficient in detecting the distant clusters. We use the second Planck catalog [1] covering 83.6% of the sky and the SPT catalog covering 2500 deg^2 [2].

The Planck catalog gives the values of y integrated over the cluster Y_{500} within the radius R_{500} , i.e the radius inside which the average density is 500 times the critical density at the redshift of the cluster, estimated from measurements of Y_{5R500} assuming a cluster model. The SPT catalog on the other hand provide the core radius (θ_c) of the beta profile fit to the cluster [81] along with the integrated y signal inside the $\theta_{\max} = 0.75'$ radius for each cluster,

$$\begin{aligned}
Y(\theta_{\max}) &= 2\pi \int_0^{\theta_{\max}} \frac{y_0 \theta d\theta}{1 + \theta^2/\theta_c^2} \\
&= \pi y_0 \theta_c^2 \log \left(1 + \frac{\theta_{\max}^2}{\theta_c^2} \right)
\end{aligned} \tag{4.1}$$

The beta profile has been previously found to be a good fit to the SPT clusters out to virial radius of $\theta_{500} \approx 5\theta_c$ [82]. We therefore integrate the y signal out to $5\theta_c$ for all SPT clusters. The average contribution of Planck and SPT clusters is given in Table 3.

For the clean Planck sample, where we remove the sources identified by our algorithm as molecular clouds [3], we get a total value of 4.3×10^{-8} which agrees beautifully with the value we estimated directly from our maps for the Planck clusters in the previous section. This shows indirectly the agreement between our y -maps and those created by the Planck collaboration. From Fig. 6 in [2] we see that most of the Planck detected clusters lie at $z < 0.3$ whereas the majority of the SPT clusters are at $z > 0.3$. We therefore use this redshift to divide both the SPT and the Planck clusters into the low redshift and high redshift samples. For the low redshift contribution to the average y -distortion we take the Planck low redshift clean sample value of $\langle y \rangle_{z \leq 0.3} = 3.3 \times 10^{-8}$. In calculating this value we have not included the clusters for which redshift is not known. Those clusters are included in the $z > 0.3$ values.

For the SPT samples, we show values calculated by extrapolating the quoted parameters in the SPT cluster to $3\theta_c$ and $5\theta_c$. For the high redshift sample, there is a difference of 30% in these two values. For our lower limit we decide to be conservative and choose the smaller value giving $\langle y \rangle_{z > 0.3} = 2.1 \times 10^{-8}$. Combining the Planck and SPT therefore we get the final lower bound on the average y distortion of $\langle y \rangle > 5.4 \times 10^{-8}$. In the published proposal of the Pixie experiment [22], the target is given as $5\text{-}\sigma$ detection of $\langle y \rangle = 10^{-8}$. Our calculations therefore guarantee that Pixie would detect an average y -type distortion at least $27\text{-}\sigma$.

5 Conclusions

We have used our recently constructed maps of y -type distortion from the Planck HFI channels to arrive at strong upper bounds on the average y -distortion or the monopole. The FFP6 simulations indicate that our value is dominated by the foregrounds contamination which drives the value higher and this bound should be considered as hard upper bound. This bound is $\langle y \rangle < 2.2 \times 10^{-6}$ and is a factor of 6.8 stronger than the COBE-FIRAS 95% upper limit of 15×10^{-6} . There is however a caveat. Our limit only applies to the contribution to the monopole from the fluctuating component of the y -type distortion, since this is the signal to which Planck is sensitive. The COBE-FIRAS measurements were on the other hand absolute measurements and also constrain the non-fluctuating or the invariant background component. The two main sources of uncertainty in our $\langle y \rangle$ are the residual foregrounds, especially the galactic CO emission, and offsets between the Planck channel maps since Planck does not measure the absolute brightness of the sky. We estimate the error in our upper limit from the systematic offsets to be $< 10^{-6}$.

We have also derived a strong lower bound on the average y -type distortion using the Planck and SPT cluster catalogues. This bound is $\langle y \rangle > 5.4 \times 10^{-8}$ and should also be considered a hard lower bound.

Our analysis predicts a very optimistic picture for the proposed experiment Pixie which should detect the global y -type distortion monopole at $\gtrsim 27\text{-}\sigma$. We of course expect the actual distortions to be much higher. With the future cluster surveys similar to current SPT, Planck and ACT, we expect to measure and remove most of the contributions from the low redshift large scale structure from the Pixie measurements and reach the invariant (non-fluctuating) y -distortion created during the reionization.

Acknowledgments

This paper used observations obtained with Planck (<http://www.esa.int/Planck>), an ESA science mission with instruments and contributions directly funded by ESA Member States, NASA, and Canada. We also acknowledge use of the HEALPix software [83] (<http://healpix.sourceforge.net>) and FFP6 simulations generated using the Planck sky model [77] http://wiki.cosmos.esa.int/planckpla/index.php/Simulation_data. This research has made use of "Aladin sky atlas" developed at CDS, Strasbourg Observatory, France [84]. This research has also made use of the SIMBAD database, operated at CDS, Strasbourg, France. We would also like to thank Jacques Delabrouille and Julian Borrill for clarifying the presence of monopole offsets in the Planck FFP simulations. RS acknowledges partial support by grant No. 14-22-00271 from the Russian Scientific Foundation.

References

- [1] Planck Collaboration, P. A. R. Ade, N. Aghanim, M. Arnaud, M. Ashdown, J. Aumont, C. Baccigalupi, A. J. Banday, R. B. Barreiro, R. Barrena, and et al. Planck 2015 results. XXVII. The Second Planck Catalogue of Sunyaev-Zeldovich Sources. *ArXiv e-prints*, February 2015. [arXiv:1502.01598](https://arxiv.org/abs/1502.01598), [ADS].
- [2] L. E. Bleem et al. Galaxy Clusters Discovered via the Sunyaev-Zel'dovich Effect in the 2500-Square-Degree SPT-SZ Survey. *ApJS*, 216:27, February 2015. [arXiv:1409.0850](https://arxiv.org/abs/1409.0850), [DOI], [ADS].
- [3] R. Khatri. An alternative validation strategy for the Planck cluster catalog and y -distortion maps. *ArXiv e-prints*, May 2015. [arXiv:1505.00778](https://arxiv.org/abs/1505.00778), [ADS].

- [4] Planck Collaboration, P. A. R. Ade, N. Aghanim, M. Arnaud, M. Ashdown, J. Aumont, C. Baccigalupi, M. Baker, A. Balbi, A. J. Banday, and et al. Planck early results. I. The Planck mission. *A&A*, 536:A1, December 2011. [arXiv:1101.2022](#), [\[DOI\]](#), [\[ADS\]](#).
- [5] D. J. Fixsen, E. S. Cheng, J. M. Gales, J. C. Mather, R. A. Shafer, and E. L. Wright. The Cosmic Microwave Background Spectrum from the Full COBE FIRAS Data Set. *ApJ*, 473:576, 1996. [\[DOI\]](#), [\[ADS\]](#).
- [6] E. L. Wright, C. L. Bennett, K. Gorski, G. Hinshaw, and G. F. Smoot. Angular Power Spectrum of the Cosmic Microwave Background Anisotropy seen by the COBE DMR. *ApJL*, 464:L21, 1996. [\[DOI\]](#), [\[ADS\]](#).
- [7] Y. B. Zeldovich and R. A. Sunyaev. The Interaction of Matter and Radiation in a Hot-Model Universe. *ApSS*, 4:301–316, 1969. [\[DOI\]](#), [\[ADS\]](#).
- [8] Planck Collaboration, N. Aghanim, M. Arnaud, M. Ashdown, J. Aumont, C. Baccigalupi, A. J. Banday, R. B. Barreiro, J. G. Bartlett, N. Bartolo, and et al. Planck 2015 results. XXII. A map of the thermal Sunyaev-Zeldovich effect. *ArXiv e-prints*, February 2015. [arXiv:1502.01596](#), [\[ADS\]](#).
- [9] J. C. Hill and D. N. Spergel. Detection of thermal SZ-CMB lensing cross-correlation in Planck nominal mission data. *JCAP*, 2:30, February 2014. [arXiv:1312.4525](#), [\[DOI\]](#), [\[ADS\]](#).
- [10] J. C. Hill, B. D. Sherwin, K. M. Smith, G. E. Addison, N. Battaglia, E. S. Battistelli, J. R. Bond, E. Calabrese, M. J. Devlin, J. Dunkley, R. Dunner, T. Essinger-Hileman, M. B. Gralla, A. Hajian, M. Hasselfield, A. D. Hincks, R. Hlozek, J. P. Hughes, A. Kosowsky, T. Louis, D. Marsden, K. Moodley, M. D. Niemack, L. A. Page, B. Partridge, B. Schmitt, N. Sehgal, J. L. Sievers, D. N. Spergel, S. T. Staggs, D. S. Swetz, R. Thornton, H. Trac, and E. J. Wollack. The Atacama Cosmology Telescope: A Measurement of the Thermal Sunyaev-Zel’dovich One-Point PDF. *ArXiv e-prints*, November 2014. [arXiv:1411.8004](#), [\[ADS\]](#).
- [11] D. Marsden, M. Gralla, T. A. Marriage, E. R. Switzer, B. Partridge, M. Massardi, G. Morales, G. Addison, J. R. Bond, D. Crichton, S. Das, M. Devlin, R. Dünner, A. Hajian, M. Hilton, A. Hincks, J. P. Hughes, K. Irwin, A. Kosowsky, F. Menanteau, K. Moodley, M. Niemack, L. Page, E. D. Reese, B. Schmitt, N. Sehgal, J. Sievers, S. Staggs, D. Swetz, R. Thornton, and E. Wollack. The Atacama Cosmology Telescope: dusty star-forming galaxies and active galactic nuclei in the Southern survey. *MNRAS*, 439:1556–1574, April 2014. [arXiv:1306.2288](#), [\[DOI\]](#), [\[ADS\]](#).
- [12] R. A. Sunyaev and Y. B. Zeldovich. The Observations of Relic Radiation as a Test of the Nature of X-Ray Radiation from the Clusters of Galaxies. *Comments on Astrophysics and Space Physics*, 4:173, 1972. [\[ADS\]](#).
- [13] L. A. Pozdnyakov, I. M. Sobol, and R. A. Sunyaev. Comptonization and the shaping of X-ray source spectra - Monte Carlo calculations. *Astrophysics and Space Physics Reviews*, 2:189–331, 1983. [\[ADS\]](#).
- [14] Z. Staniszewski et al. Galaxy Clusters Discovered with a Sunyaev-Zel’dovich Effect Survey. *ApJ*, 701:32–41, August 2009. [arXiv:0810.1578](#), [\[DOI\]](#), [\[ADS\]](#).
- [15] R. J. Foley et al. Discovery and Cosmological Implications of SPT-CL J2106-5844, the Most Massive Known Cluster at $z > 1$. *ApJ*, 731:86, April 2011. [arXiv:1101.1286](#), [\[DOI\]](#), [\[ADS\]](#).
- [16] T. Marriage et al. The Atacama Cosmology Telescope: Sunyaev-Zel’dovich-Selected Galaxy Clusters at 148 GHz in the 2008 Survey. *ApJ*, 737:61, August 2011. [arXiv:1010.1065](#), [\[DOI\]](#), [\[ADS\]](#).
- [17] F. Menanteau et al. The Atacama Cosmology Telescope: ACT-CL J0102-4915 ”El Gordo,” a Massive Merging Cluster at Redshift 0.87. *ApJ*, 748:7, March 2012. [arXiv:1109.0953](#), [\[DOI\]](#), [\[ADS\]](#).
- [18] M. Hasselfield et al. The Atacama Cosmology Telescope: Sunyaev-Zel’dovich selected galaxy clusters at 148 GHz from three seasons of data. *JCAP*, 7:8, July 2013. [arXiv:1301.0816](#), [\[DOI\]](#), [\[ADS\]](#).
- [19] C. L. Reichardt et al. Galaxy Clusters Discovered via the Sunyaev-Zel’dovich Effect in the First 720 Square Degrees of the South Pole Telescope Survey. *ApJ*, 763:127, February 2013. [arXiv:1203.5775](#), [\[DOI\]](#), [\[ADS\]](#).

- [20] Planck Collaboration, P. A. R. Ade, N. Aghanim, C. Armitage-Caplan, M. Arnaud, M. Ashdown, F. Atrio-Barandela, J. Aumont, H. Aussel, C. Baccigalupi, and et al. Planck 2013 results. XXIX. The Planck catalogue of Sunyaev-Zeldovich sources. *A&A*, 571:A29, November 2014. [arXiv:1303.5089](#), [\[DOI\]](#), [\[ADS\]](#).
- [21] Planck Collaboration, P. A. R. Ade, N. Aghanim, M. Arnaud, M. Ashdown, J. Aumont, C. Baccigalupi, A. J. Banday, R. B. Barreiro, J. G. Bartlett, and et al. Planck 2015 results. XIII. Cosmological parameters. *ArXiv e-prints*, February 2015. [arXiv:1502.01589](#), [\[ADS\]](#).
- [22] A. Kogut, D. J. Fixsen, D. T. Chuss, J. Dotson, E. Dwek, M. Halpern, G. F. Hinshaw, S. M. Meyer, S. H. Moseley, M. D. Seiffert, D. N. Spergel, and E. J. Wollack. The Primordial Inflation Explorer (PIXIE): a nulling polarimeter for cosmic microwave background observations. *JCAP*, 7:25, 2011. [\[DOI\]](#), [\[ADS\]](#).
- [23] P. Andre et al. PRISM (Polarized Radiation Imaging and Spectroscopy Mission): an extended white paper. *JCAP*, 2:6, February 2014. [arXiv:1310.1554](#), [\[DOI\]](#), [\[ADS\]](#).
- [24] D. J. Fixsen and J. C. Mather. The Spectral Results of the Far-Infrared Absolute Spectrophotometer Instrument on COBE. *ApJ*, 581:817–822, 2002. [\[DOI\]](#), [\[ADS\]](#).
- [25] J. Mather. From the Big Bang to the Nobel Prize and the James Webb Space Telescope. *Nuovo Cimento B Serie*, 122:1315–1326, December 2007. [\[DOI\]](#), [\[ADS\]](#).
- [26] J. Silk. Cosmic Black-Body Radiation and Galaxy Formation. *ApJ*, 151:459, 1968. [\[DOI\]](#), [\[ADS\]](#).
- [27] P. J. E. Peebles and J. T. Yu. Primeval Adiabatic Perturbation in an Expanding Universe. *ApJ*, 162:815, 1970. [\[DOI\]](#), [\[ADS\]](#).
- [28] N. Kaiser. Small-angle anisotropy of the microwave background radiation in the adiabatic theory. *MNRAS*, 202:1169–1180, 1983. [\[ADS\]](#).
- [29] A. G. Doroshkevich, Y. B. Zeldovich, and R. A. Sunyaev. Fluctuations of the microwave background radiation in the adiabatic and entropic theories of galaxy formation. *Soviet Astronomy*, 22:523–528, October 1978. [\[ADS\]](#).
- [30] R. Keisler et al. A Measurement of the Damping Tail of the Cosmic Microwave Background Power Spectrum with the South Pole Telescope. *ApJ*, 743:28, 2011. [\[DOI\]](#), [\[ADS\]](#).
- [31] R. Hlozek et al. The Atacama Cosmology Telescope: A Measurement of the Primordial Power Spectrum. *ApJ*, 749:90, 2012. [\[DOI\]](#), [\[ADS\]](#).
- [32] Planck collaboration, P. A. R. Ade, N. Aghanim, C. Armitage-Caplan, M. Arnaud, and et al. Planck 2013 results. XV. CMB power spectra and likelihood. *arxiv:1303.5075*, March 2013. [\[ADS\]](#).
- [33] R. A. Sunyaev and Y. B. Zeldovich. The interaction of matter and radiation in the hot model of the Universe, II. *ApSS*, 7:20–30, 1970. [\[DOI\]](#), [\[ADS\]](#).
- [34] J. Chluba, R. Khatri, and R. A. Sunyaev. CMB at 2×2 order: the dissipation of primordial acoustic waves and the observable part of the associated energy release. *MNRAS*, 425:1129–1169, 2012. [\[DOI\]](#), [\[ADS\]](#).
- [35] R. Khatri, R. A. Sunyaev, and J. Chluba. Mixing of blackbodies: entropy production and dissipation of sound waves in the early Universe. *A&A*, 543:A136, 2012. [\[DOI\]](#), [\[ADS\]](#).
- [36] A. F. Illarionov and R. A. Sunyaev. Comptonization, characteristic radiation spectra, and thermal balance of low-density plasma. *Soviet Astronomy*, 18:413–419, 1975. [\[ADS\]](#).
- [37] A. F. Illarionov and R. A. Sunyaev. Comptonization, the background-radiation spectrum, and the thermal history of the universe. *Soviet Astronomy*, 18:691–699, 1975. [\[ADS\]](#).
- [38] W. Hu and J. Silk. Thermalization and spectral distortions of the cosmic background radiation. *Phys.Rev.D*, 48:485–502, 1993. [\[DOI\]](#), [\[ADS\]](#).
- [39] J. Silk and A. Stebbins. Decay of long-lived particles in the early universe. *ApJ*, 269:1–12, June 1983. [\[DOI\]](#), [\[ADS\]](#).

- [40] C. Burigana, L. Danese, and G. de Zotti. Formation and evolution of early distortions of the microwave background spectrum - A numerical study. *A&A*, 246:49–58, 1991. [\[ADS\]](#).
- [41] P. Procopio and C. Burigana. A numerical code for the solution of the Kompaneets equation in cosmological context. *A&A*, 507:1243–1256, 2009. [\[DOI\]](#), [\[ADS\]](#).
- [42] J. Chluba and R. A. Sunyaev. The evolution of CMB spectral distortions in the early Universe. *MNRAS*, 419:1294–1314, 2012. [\[DOI\]](#), [\[ADS\]](#).
- [43] R. Khatri and R. A. Sunyaev. Beyond y and μ : the shape of the CMB spectral distortions in the intermediate epoch, $1.5 \times 10^4 \lesssim z \lesssim 2 \times 10^5$. *JCAP*, 9:16, 2012. [\[DOI\]](#), [\[ADS\]](#).
- [44] R. Khatri and R. A. Sunyaev. Forecasts for CMB μ - and i -type spectral distortion constraints on the primordial power spectrum on scales $8 \lesssim k \lesssim 10^4 \text{Mpc}^{-1}$ with the future Pixie-like experiments. *ArXiv e-prints*, March 2013. [arXiv:1303.7212](#), [\[ADS\]](#).
- [45] E. Pajer and M. Zaldarriaga. New Window on Primordial Non-Gaussianity. *Physical Review Letters*, 109(2):021302, 2012. [\[DOI\]](#), [\[ADS\]](#).
- [46] J. Ganc and E. Komatsu. Scale-dependent bias of galaxies and μ -type distortion of the cosmic microwave background spectrum from single-field inflation with a modified initial state. *Phys.Rev.D*, 86(2):023518, 2012. [\[DOI\]](#), [\[ADS\]](#).
- [47] R. Emami, E. Dimastrogiovanni, J. Chluba, and M. Kamionkowski. Probing the scale dependence of non-Gaussianity with spectral distortions of the cosmic microwave background. *ArXiv e-prints*, April 2015. [arXiv:1504.00675](#), [\[ADS\]](#).
- [48] X. Chen and M. Kamionkowski. Particle decays during the cosmic dark ages. *Phys.Rev.D*, 70(4):043502, August 2004. [arXiv:astro-ph/0310473](#), [\[DOI\]](#), [\[ADS\]](#).
- [49] N. Padmanabhan and D. P. Finkbeiner. Detecting dark matter annihilation with CMB polarization: Signatures and experimental prospects. *Phys.Rev.D*, 72(2):023508, July 2005. [arXiv:astro-ph/0503486](#), [\[DOI\]](#), [\[ADS\]](#).
- [50] T. R. Slatyer, N. Padmanabhan, and D. P. Finkbeiner. CMB constraints on WIMP annihilation: Energy absorption during the recombination epoch. *Phys.Rev.D*, 80(4):043526, 2009. [\[DOI\]](#), [\[ADS\]](#).
- [51] G. Hütsi, J. Chluba, A. Hektor, and M. Raidal. WMAP7 and future CMB constraints on annihilating dark matter: implications for GeV-scale WIMPs. *A&A*, 535:A26, November 2011. [arXiv:1103.2766](#), [\[DOI\]](#), [\[ADS\]](#).
- [52] R. Khatri and R. A. Sunyaev. Creation of the CMB spectrum: precise analytic solutions for the blackbody photosphere. *JCAP*, 6:38, 2012. [\[DOI\]](#), [\[ADS\]](#).
- [53] R. Barkana and A. Loeb. In the beginning: the first sources of light and the reionization of the universe. *Physics Reports*, 349:125–238, July 2001. [arXiv:astro-ph/0010468](#), [\[DOI\]](#), [\[ADS\]](#).
- [54] R. A. Sunyaev and Y. B. Zeldovich. Small-Scale Fluctuations of Relic Radiation. *ApSS*, 7:3–19, 1970. [\[DOI\]](#), [\[ADS\]](#).
- [55] R. A. Sunyaev and Y. B. Zeldovich. Formation of Clusters of Galaxies; Protocluster Fragmentation and Intergalactic Gas Heating. *A&A*, 20:189, August 1972. [\[ADS\]](#).
- [56] R. Cen and J. P. Ostriker. Where Are the Baryons? *ApJ*, 514:1–6, 1999. [\[DOI\]](#), [\[ADS\]](#).
- [57] A. Refregier, E. Komatsu, D. N. Spergel, and U.-L. Pen. Power spectrum of the Sunyaev-Zel’dovich effect. *Phys.Rev.D*, 61(12):123001, June 2000. [arXiv:astro-ph/9912180](#), [\[DOI\]](#), [\[ADS\]](#).
- [58] V. Springel, M. White, and L. Hernquist. Hydrodynamic Simulations of the Sunyaev-Zeldovich Effect(s). *ApJ*, 549:681–687, March 2001. [arXiv:astro-ph/0008133](#), [\[DOI\]](#), [\[ADS\]](#).
- [59] V. Springel, M. White, and L. Hernquist. Erratum: Hydrodynamic Simulations of the Sunyaev-Zeldovich Effect(s). *ApJ*, 562:1086–1086, December 2001. [\[DOI\]](#), [\[ADS\]](#).

- [60] B. B. Nath and J. Silk. Heating of the intergalactic medium as a result of structure formation. *MNRAS*, 327:L5–L9, 2001. [\[DOI\]](#), [\[ADS\]](#).
- [61] M. White, L. Hernquist, and V. Springel. Simulating the Sunyaev-Zeldovich Effect(s): Including Radiative Cooling and Energy Injection by Galactic Winds. *ApJ*, 579:16–22, November 2002. [arXiv:astro-ph/0205437](#), [\[DOI\]](#), [\[ADS\]](#).
- [62] B. M. Schäfer, C. Pfrommer, M. Bartelmann, V. Springel, and L. Hernquist. Detecting Sunyaev-Zel’dovich clusters with Planck - I. Construction of all-sky thermal and kinetic SZ maps. *MNRAS*, 370:1309–1323, August 2006. [arXiv:astro-ph/0407089](#), [\[DOI\]](#), [\[ADS\]](#).
- [63] L. D. Shaw, D. Nagai, S. Bhattacharya, and E. T. Lau. Impact of Cluster Physics on the Sunyaev-Zel’dovich Power Spectrum. *ApJ*, 725:1452–1465, December 2010. [arXiv:1006.1945](#), [\[DOI\]](#), [\[ADS\]](#).
- [64] N. Battaglia, J. R. Bond, C. Pfrommer, J. L. Sievers, and D. Sijacki. Simulations of the Sunyaev-Zel’dovich Power Spectrum with Active Galactic Nucleus Feedback. *ApJ*, 725:91–99, December 2010. [arXiv:1003.4256](#), [\[DOI\]](#), [\[ADS\]](#).
- [65] N. Battaglia, J. R. Bond, C. Pfrommer, and J. L. Sievers. On the Cluster Physics of Sunyaev-Zel’dovich and X-Ray Surveys. II. Deconstructing the Thermal SZ Power Spectrum. *ApJ*, 758:75, October 2012. [arXiv:1109.3711](#), [\[DOI\]](#), [\[ADS\]](#).
- [66] D. Munshi, S. Joudaki, J. Smidt, P. Coles, and S. T. Kay. Statistical properties of thermal Sunyaev-Zel’dovich maps. *MNRAS*, 429:1564–1584, February 2013. [arXiv:1106.0766](#), [\[DOI\]](#), [\[ADS\]](#).
- [67] K. Dolag and R. Sunyaev. Relative velocity of dark matter and baryons in clusters of galaxies and measurements of their peculiar velocities. *MNRAS*, 432:1600–1615, June 2013. [\[DOI\]](#), [\[ADS\]](#).
- [68] K. Dolag, R. Sunyaev, and E. Komatsu. The thermal sunyaev-zeldovich power spectrum from the magneticum pathfinder simulation. *to be submitted*, 2015.
- [69] S. L. Snowden, R. Egger, D. P. Finkbeiner, M. J. Freyberg, and P. P. Plucinsky. Progress on Establishing the Spatial Distribution of Material Responsible for the 1–4 keV Soft X-Ray Diffuse Background Local and Halo Components. *ApJ*, 493:715–729, January 1998. [\[DOI\]](#), [\[ADS\]](#).
- [70] A. Gupta, S. Mathur, Y. Krongold, F. Nicastro, and M. Galeazzi. A Huge Reservoir of Ionized Gas around the Milky Way: Accounting for the Missing Mass? *ApJL*, 756:L8, September 2012. [arXiv:1205.5037](#), [\[DOI\]](#), [\[ADS\]](#).
- [71] G. Hurier, J. F. Macías-Pérez, and S. Hildebrandt. MILCA, a modified internal linear combination algorithm to extract astrophysical emissions from multifrequency sky maps. *A&A*, 558:A118, October 2013. [arXiv:1007.1149](#), [\[DOI\]](#), [\[ADS\]](#).
- [72] J. Delabrouille, J.-F. Cardoso, M. Le Jeune, M. Betoule, G. Fay, and F. Guillaux. A full sky, low foreground, high resolution CMB map from WMAP. *A&A*, 493:835–857, January 2009. [arXiv:0807.0773](#), [\[DOI\]](#), [\[ADS\]](#).
- [73] R. Khatri. Linearized iterative least-squares (LIL): A parameter fitting algorithm for component separation in multifrequency CMB experiments such as Planck. *ArXiv e-prints*, October 2014. [arXiv:1410.7396](#), [\[ADS\]](#).
- [74] M. Righi, C. Hernández-Monteagudo, and R. A. Sunyaev. Carbon monoxide line emission as a CMB foreground: tomography of the star-forming universe with different spectral resolutions. *A&A*, 489:489–504, October 2008. [arXiv:0805.2174](#), [\[DOI\]](#), [\[ADS\]](#).
- [75] Planck Collaboration, P. A. R. Ade, N. Aghanim, C. Armitage-Caplan, M. Arnaud, M. Ashdown, F. Atrio-Barandela, J. Aumont, C. Baccigalupi, A. J. Banday, and et al. Planck 2013 results. IX. HFI spectral response. *ArXiv e-prints*, March 2013. [arXiv:1303.5070](#), [\[ADS\]](#).

- [76] J. A. Rubiño-Martín and R. A. Sunyaev. Discriminating between unresolved point sources and ‘negative’ Sunyaev-Zel’dovich clusters in cosmic microwave background maps. *MNRAS*, 344:1155–1174, October 2003. [arXiv:astro-ph/0211430](#), [DOI], [ADS].
- [77] J. Delabrouille et al. The pre-launch Planck Sky Model: a model of sky emission at submillimetre to centimetre wavelengths. *A&A*, 553:A96, May 2013. [arXiv:1207.3675](#), [DOI], [ADS].
- [78] Planck Collaboration, R. Adam, P. A. R. Ade, N. Aghanim, M. Arnaud, M. Ashdown, J. Aumont, C. Baccigalupi, A. J. Banday, R. B. Barreiro, and et al. Planck 2015 results. VIII. High Frequency Instrument data processing: Calibration and maps. *ArXiv e-prints*, February 2015. [arXiv:1502.01587](#), [ADS].
- [79] Planck Collaboration, R. Adam, P. A. R. Ade, N. Aghanim, M. I. R. Alves, M. Arnaud, M. Ashdown, J. Aumont, C. Baccigalupi, A. J. Banday, and et al. Planck 2015 results. X. Diffuse component separation: Foreground maps. *ArXiv e-prints*, February 2015. [arXiv:1502.01588](#), [ADS].
- [80] Planck Collaboration, P. A. R. Ade, N. Aghanim, C. Armitage-Caplan, M. Arnaud, M. Ashdown, F. Atrio-Barandela, J. Aumont, C. Baccigalupi, A. J. Banday, and et al. Planck 2013 results. VIII. HFI photometric calibration and mapmaking. *A&A*, 571:A8, November 2014. [arXiv:1303.5069](#), [DOI], [ADS].
- [81] A. Cavaliere and R. Fusco-Femiano. X-rays from hot plasma in clusters of galaxies. *A&A*, 49:137–144, May 1976. [ADS].
- [82] T. Plagge et al. Sunyaev-Zel’dovich Cluster Profiles Measured with the South Pole Telescope. *ApJ*, 716:1118–1135, June 2010. [arXiv:0911.2444](#), [DOI], [ADS].
- [83] K. M. Górski, E. Hivon, A. J. Banday, B. D. Wandelt, F. K. Hansen, M. Reinecke, and M. Bartelmann. HEALPix: A Framework for High-Resolution Discretization and Fast Analysis of Data Distributed on the Sphere. *ApJ*, 622:759–771, April 2005. [arXiv:astro-ph/0409513](#), [DOI], [ADS].
- [84] F. Bonnarel, P. Fernique, O. Bienaymé, D. Egret, F. Genova, M. Louys, F. Ochsenbein, M. Wenger, and J. G. Bartlett. The ALADIN interactive sky atlas. A reference tool for identification of astronomical sources. *A&A Supp.*, 143:33–40, April 2000. [DOI], [ADS].